The Journal of Adhesion

Peel-Zone Model of Tape Peeling Based on the Gecko
Adhesive System

PLEASE SCROLL DOWN FOR ARTICLE

Taylor & Francis
Taylor & Francis Group

Peel-Zone Model of Tape Peeling Based on the Gecko Adhesive System

Noshir S. Pesika
Department of Chemical Engineering and California NanoSystems Institute (CNSI), University of California, Santa Barbara, California, USA

Yu Tian
Department of Chemical Engineering and California NanoSystems Institute (CNSI), University of California, Santa Barbara, California, USA and State Key Laboratory of Tribology, Department of Precision Instruments, Tsinghua University, Beijing, China

Boxin Zhao
Kenny Rosenberg
Hongbo Zeng
Patricia McGuiggan
Department of Chemical Engineering and California NanoSystems Institute (CNSI), University of California, Santa Barbara, California, USA

Kellar Autumn
Department of Biology, Lewis and Clark College, Portland, Oregan, USA

Jacob N. Israelachvili
Department of Chemical Engineering and California NanoSystems Institute (CNSI), University of California, Santa Barbara, California, USA

383

A tape-peeling model based on the geometry of the peel zone (PZ) is derived to predict the peeling behavior of adhesive tapes at peel angles less than or equal to 90°. The PZ model adds an angle-dependent multiplier to the Kendall equation that takes into account the geometrical changes within the peel zone. The model is compared with experimental measurements of the peel force at different angles for a model tape and two commercial tapes, each with different bending moduli, stretch moduli, and adhesive strengths. Good agreement is found for a wide range of peel angles. The PZ model is also applied to the gecko adhesive system and predicts a spatula peel angle of 18.4° to achieve the adhesion forces reported for single setae. The PZ model captures the fact that adhesive forces can be significantly enhanced by peeling at an angle, thereby exploiting high friction forces between the detaching material and the substrate.

INTRODUCTION

Understanding how geckos derive a high adhesion and friction force from their adhesive pads and the role of geometry is essential for the design of dry adhesives. Autumn *et al.* [1,2] were the first to show that the relatively weak van der Waals forces are responsible for strong gecko adhesion. This is due to the complex hierarchical structure (geometry) of the gecko foot, coupled to the compliances of the different components of the adhesive system [3], which allows for intimate contact of the adhesive pads to almost any surface. In addition, the way these hierarchical structures are articulated (*e.g.,* their configuration and angles at which they are pulled, shown in Figure 1a) result in large adhesion forces, $F_\perp$, acting normal to the surface. The fact that van der Waals forces are always present between any two surfaces in contact has motivated the fabrication of dry adhesives inspired by the gecko adhesive system [4,5]. Geckos further enhance the adhesion of the adhesive pads by exploiting the high friction forces $F_\parallel$—again due to van der Waals forces—acting parallel to the surface [see Eq. (7)]. The biomechanics of a gecko walking on a surface [6,7] reveals the use of a particular configuration, referred to here as the *Y-configuration* (Figure 1b). In this configuration, to make a step forward, the gecko always has two diagonally opposite feet on the surface while detaching the other two, as shown in Figure 1a. The two attached feet (front right and back left feet in Figure 1a) are angled to the surface at an angle, θ, with a tension, F, along the feet, making a Y-shaped geometry and yielding a total force $F_{total} = 2\,F_\perp$ in the normal direction to the surface. The Y-shaped geometry was also reported by Autumn *et al.* [8] in which it was found that the opposing feet of the gecko were pulling inward toward the center of mass. The peel test schematically
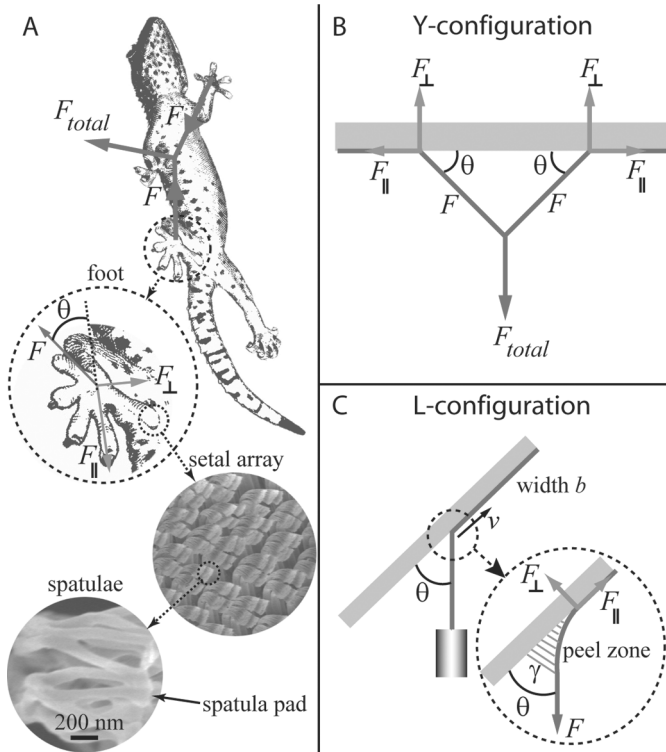
FIGURE 1 (a) Ventral view of a gecko walking on a glass surface. Each toe is composed of a hierarchical level of structures; the setae are approximately 100 μm in length × 5 μm in diameter keratin-based pillars that originate from the gecko toe skin and split into 100–1000 spatulae (triangular keratin-based adhesive structures that make up the final hierarchical level of the gecko adhesive system structures; they are approximately 200 nm at the base narrowing to ~100 nm and 10 nm in thickness). (b) Schematic of the Y-configuration showing a force balance between the tape and the surface. (c) Schematic of the L-configuration used in peel tests showing the different forces in the peel zone.

shown in Figure 1c, referred to here as the *L-configuration*, is a common test used to characterize the peeling behavior of adhesive tapes and was used here to study the gecko adhesive system, specifically at the spatula level (see Figure 1), while the animal is at rest or in motion. The use of PSAs in our study allows for intimate contact between the adhesive and the substrate analogous to the gecko adhesive system, in which the intimate contact is achieved by the final fine structures (*i.e.,* the spatulae pads).

Many complex models have been proposed to describe the peeling behavior of adhesive tapes [9–17]. One of the most commonly used models was first proposed by Rivlin [9] and modified by Kendall [10] to include the elastic energy of the tape backing. The Kendall equation, Eq. (1), originally applied to the detachment of a thin elastomeric film from a rigid surface, is widely used and has been confirmed by numerous experiments [18,19]. Previous studies of gecko adhesion [20–23] have modeled the adhesive pads of geckos as nanoscale strips of tape. For the geometry shown in Figure 1c, the Kendall equation for the peel force is [10]

$$\frac{F}{b} = \frac{\gamma}{(1 - \cos\theta)} + \text{elastic energy term}, \qquad (1)$$

where F is the peel force in the peeling direction, b is the tape width, γ is the adhesion energy, and θ is the peel angle. The Kendall equation (neglecting the elastic energy term of the tape backing) is derived based on an energy balance by considering the adhesive force between the tape and the surface and the amount of energy required to peel the tape to a new location while at a constant peel angle, θ. The Kendall equation inherently does not provide any information about the geometry of the peel zone nor how friction forces contribute to the adhesion force.

Frictional energy losses due to interfacial slip between an adhesive layer and a substrate has previously been studied [24,25], although the influence of the peel angle on the peel force was not considered. In previous work [26], we performed a molecular-level analysis to estimate the pulling force generated by the adhesion and friction of a single spatula by considering van der Waals forces between the adhering surfaces. In this article, we use a macroscopic analysis (*i.e.*, tape peeling) to model the adhesion of a single gecko spatula.

THEORY

We derive a new quantitative model for tape peeling based on the geometry of the peel zone (PZ model), as ascertained from microscopic observations of the peel zone during detachment, as described later. The PZ model is derived based on a force balance at the peel zone and takes into account three forces: the peel force F acting in the peel direction, the adhesion force $F_\perp$ acting normal to the surface, and the friction/shear force $F_\parallel$ acting parallel to the surface. Although energy balances have been used in the past [10–12,17,18,24] to describe the peeling of adhesives tapes, energy losses in the system during detachment are often not considered because of the nontrivial description of

these energies and the fact that the forces act in multiple regions within the system. The friction force, $F_\parallel$, can either be dynamic, in which case one of the surfaces is sliding over the other, or static, in which case the surfaces do not move. In either case, the friction force is balanced by the parallel component of the pulling force. The peel zone is defined as the bifurcation between the tape backing and the surface in which cavitation and fibrillation occur (Figure 1c) [27–35]. We assume that the curvature of the tape backing is approximately circular in the all-important local region of the peel zone, that the distribution of forces provided by the filaments in the peel zone can be simplified to an average force, and that the length of the peel zone on the surface is equal to the arc length of the tape backing up to the point of the last fibril or filament. We also assume that the tape is composed of a backing material that has a large stretch modulus (*i.e.*, the tape does not stretch significantly). As the peel angle gets smaller, a larger fraction of the peel force F is opposed by the friction/shear force $F_\parallel$ provided by the surface. The friction force "pins" the contact end of the peel zone (using a Lagrangian reference coordinate system that moves at the same velocity, v, as the peel front), thereby increasing the radius of curvature, R, of the tape backing as shown later in Figure 2 and described by Eq. (11). The increased radius of curvature, R, increases the length of the peel zone, which in turn increases the peel force, F, in the peel direction, θ. We do not consider the variation of the filament strengths as a function of the filament lengths in this model but instead assume that the peel zone provides an average adhesive tensile force. Figure 2 shows a schematic of the peel zone for two peel regimes: peel angles between cases I and II (constant peel-zone regime), and between cases II and III (variable peel-zone regime). In the constant peel-zone regime, the geometry of the peel zone (*i.e.*, the length of the peel zone and the curvature of the tape backing) remains constant while the peel angle, θ, is changed. In contrast, in the variable peel-zone regime, the length of the peel zone and the curvature of the tape baking both increase as the peel angle, θ is changed. The peel-zone region is bounded by the leading edge and the stationary point (the location of the last active filament). The stationary point is assumed to remain at the same normal distance from the detaching surface for all peel angles because it is determined by the (constant) tensile force of the last active filament. The normal component of the peel force $F_\perp$ is proportional to the area of the peel zone,

$$F_\perp \propto Sb, \qquad \text{or } F_\perp = CSb, \qquad (2)$$

where S is the length of the peel zone, b is the width of the tape, and C is a constant multiplier. The adhesion energy, γ, of the tape detachment
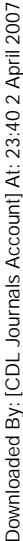
FIGURE 2 Schematic illustration of the peel zone showing the two peel regimes: constant peel-zone regime and variable peel-zone regime.

is defined for a 90° peel angle for which the length of the peel zone is S_o, where

$$\frac{F_\perp}{b} = \gamma = CS_o, \tag{3}$$

so that

$$C = \frac{\gamma}{S_o}. \tag{4}$$

Solving and substituting the constant C into Eq. (2) gives the normal peel force per unit width of tape:

$$\frac{F_\perp}{b} = CS = \frac{\gamma}{S_o}S. \tag{5}$$

The total peel force per unit width of tape F/b as a function of the peel angle, θ is, therefore, $F/b = F_\perp/b \sin \theta$.

Constant Peel-Zone Detachment Mode

For a tape backing with a finite bending modulus, E, the last active filament spans an angle, ϕ_o, along the tape backing (see Figure 2). An experimentally determined angle, ϕ_o, is an intrinsic property of the tape backing, adhesive, and substrate system. Depending of the tackiness of the adhesive [27–35], ϕ_o can range from $90°$ (large tackiness) to almost $0°$ (small tackiness). For peel angles greater than ϕ_o, the shape and dimension of the peel zone remains constant, and thus, the normal component of the peel force also remains constant. In this case, Eq. (5) reduces to $F_\perp/b = \gamma$, and the peel force per unit width of tape reduces to

$$\frac{F}{b} = \frac{\gamma}{\sin \theta}. \tag{6}$$

Alternatively, Eq. (6) can be derived by considering a force balance at the peel zone. As shown in Figure 1c, the peel force, F, at a peel angle, θ, is balanced by contributions from the adhesion component, $F_\perp$, and the friction/shear component, $F_\parallel$, which are related by

$$F = F_\perp \sin \theta + F_\parallel \cos \theta. \tag{7}$$

In addition, the relationship between the adhesion and friction/shear components is $\tan \theta = F_\perp/F_\parallel$. Substituting the latter into Eq. (7) yields

$$F = \frac{F_\perp}{\sin \theta}, \tag{8}$$

which when combined with Eq. (3) gives Eq. (6).

Variable Peel-Zone Detachment Mode

As the peel angle, θ, approaches, ϕ_o, the shape and dimension of the peel zone change gradually from the constant peel-zone detachment mode to the variable peel-zone detachment mode. Here we assume that this change occurs abruptly when the peel angle reaches ϕ_o. At this point, the length of the peel zone is given by

$$S_o = R_o \phi_o, \tag{9}$$

where R_o is the radius of curvature of the tape backing at $\theta = \phi_o$. As the peel angle decreases further, the new length of the peel zone changes to

$$S = R\theta, \tag{10}$$

where $\theta < \phi_o$ and where R is the new radius of curvature of the tape backing at the peel angle θ. Using simple trigonometric relationships, it can be shown that

$$\frac{R}{R_o} = \frac{1 - \cos \phi_o}{1 - \cos \theta}.$$

(11)

By substituting this relationship into Eq. (5), the peel force for the variable peel-zone detachment mode is given by

$$\frac{F(\theta, \phi_o)}{b} = \gamma \left[\frac{\theta}{\phi_o} \right] \left[\frac{1 - \cos \phi_o}{1 - \cos \theta} \right] \left[\frac{1}{\sin \theta} \right].$$

(12)

The reference adhesion energy, γ, is defined when $\theta = \phi_0$. In this case, Eq. (12) reduces to

$$\frac{F}{b} = \frac{\gamma}{\sin \phi_o}.$$

(13)

Solving for γ yields

$$\gamma = \frac{F \sin \phi_o}{b}.$$

(14)

In the special case in which the tape backing is sufficiently compliant and the curvature of the backing is dictated solely by the adhesive layer (for example, an adhesive with high tack), $\phi_0 = 90°$, and Eq. (12) reduces to

$$\frac{F}{b} = \frac{2\gamma\theta}{\pi(1 - \cos \theta) \sin \theta}.$$

(15)

The reference adhesion energy defined at $\theta = \phi_0 = 90°$ peel is now given by

$$\gamma = \frac{F}{b}.$$

(16)

The PZ model differs from the Kendall equation [*cf.* Eq. (12) and (1)] by an angle-dependent multiplier, which takes into account the increase in the length of the peel zone, S, as the peel angle is reduced. This factor causes the peel force predicted by the PZ model to be always smaller than the value given by the Kendall equation, the largest difference occurring at smaller peel angles.

EXPERIMENTAL

A model tape was created by using a double-sided tacky adhesive transfer tape (3M #950, 0.13-mm adhesive thickness, 3M, St. Paul, MN, USA) as the adhesive layer and a transparency sheet (3M Write-on Transparency film, 0.1 mm in thickness, 3M, St. Paul, MN, USA) as the stiff tape backing. The transfer tape was adhered to the transparency sheet using a hand roller (4.5 lb, 2.04 kg, ChemInstruments Inc., Fairfield, OH, USA). To ensure maximum adhesion between the transparency film and the transfer tape, the model tape was not used until the following day. The model tape was then cut into 1/4-inch (0.635-cm)-wide and 12-inch (30.48-cm)-long strips. A glass surface [Borosilicate 1/4 inch (.635 cm) $\times$ 12 inch (30.48 cm) $\times$ 6 inch (15.24 cm), McMaster-Carr, Santa Fe Springs, CA, USA] was used as the substrate surface in the peeling test. The surface was cleaned three times with diacetone alcohol (purity 99%, Sigma Aldrich, St. Louis, MO, USA) followed by three times with acetone (ACS grade, EMD) using Kimwipes (Kimtech Science, Newtown Square, PA, USA) between each cleaning to remove the solvent. All chemicals were used as received. In addition, two commercial adhesives tapes, 3M Scotch^{TM} tape [MultiTask, 3/4 inch (1.905 cm), 3M, St. Paul, MN, USA) and 3M Electrical tape [Professional Grade, Vinyl Electrical Tape, Super 33+, 3/4 inch (1.905 cm), 3M, St. Paul, MN, USA] were used in this study.
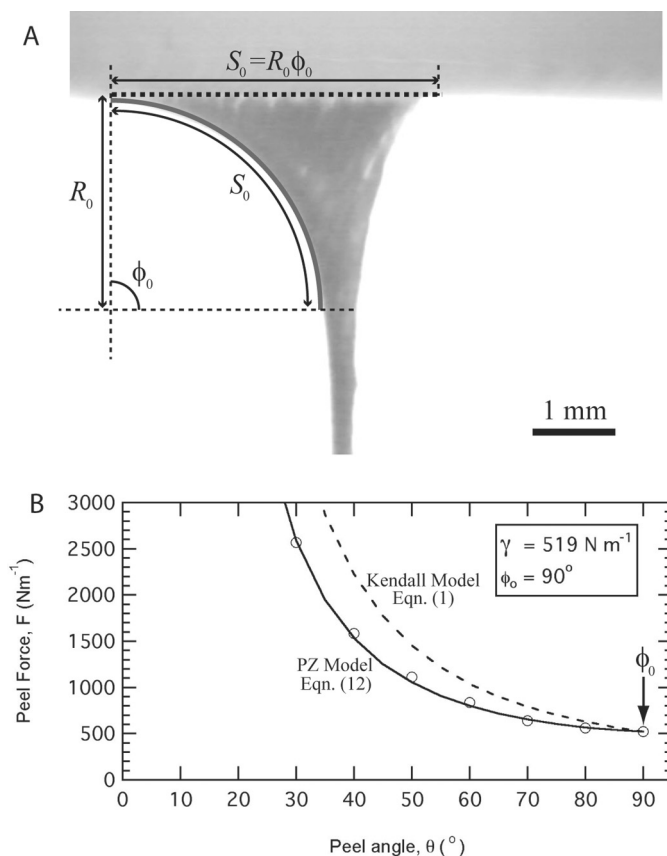
The 12-inch (30.48-cm)-long strips of tape were attached to the glass surface using a rolling cylinder to prevent entrapment of air between the glass and adhesive. A 4.5-lb (2.04-kg) hand roller was then used three times in each direction to ensure complete and uniform contact between the adhesive tape and glass. Peeling experiments were started after 1 h and 4 h of allowing the tape to be in contact with the glass at room temperature (23°C) for the model tape and commercial tapes, respectively. A schematic of the experimental setup is shown in Figure 1c. The glass surface was positioned at a predetermined angle, θ, and the peel force, F, was varied (using brass weights) to attain a desired tape detachment velocity, v, of approximately 0.03 mm/s for the model tape and 0.5 mm/s for the commercial tapes. In each experiment using the commercial tapes, the tape was allowed to reach a steady detachment velocity, v (typically after ~1 cm of peeling), before v was measured. Videos of the model tape peeling during the experiments were obtained using a monochrome camera (Pulnix, San Jose, CA, USA) with a $10 \times$ objective. Still images were obtained from the videos, and image processing (Adobe Photoshop) was performed to obtain the well-defined edges found in

Figure 4. All experiments were run under ambient humidity and temperatures between 23°C and 24°C.

RESULTS AND DISCUSSION

Because the transfer tape used to create the model tape is tacky, it allowed for the formation and visualization of relatively long filaments in the peel zone. Although the tape backing was relatively thick (0.1-mm-thick transparency film), which increased the bending modulus E, the high adhesive strength of the transfer tape still determined the curvature of the tape and backing. In addition, the backing had a high stretch modulus, which is a prerequisite for the model and is also a relevant model system for the gecko adhesive system because the spatula pads in geckos are composed of β-keratin, which is very stiff, with a Young's modulus of approximately 1.5 GPa [36]. The tape detachment velocity, v, of approximately 0.03 mm/s allowed for the adhesive failure of the tape, and therefore, no noticeable adhesive material from the tape was transferred to the substrate. The last active filament of the transfer tape spans an angle of $\phi_o \approx 90°$, as shown in Figure 3a. Figure 3b shows a plot of the measured peel force for the detachment of the model tape from the borosilicate glass surface as a function of the peel angle θ in the range 30–90°. Using Eq. (12) for $\phi_o = 90°$, the model (solid line) accurately predicts the peeling behavior of the tape within the range of angles studied. The adhesion energy, γ, defined at $\theta = 90°$, is $519 \, \mathrm{Nm}^{-1}$ as determined by Eq. (14). The reported value for the adhesion strength of the same transfer tape to steel is $820 \, \mathrm{Nm}^{-1}$. Note that the adhesion energy, γ, is not equal to the thermodynamic surface energy but is depended on tape backing, adhesive, substrate, and detachment velocity, v. For comparison, the Kendall equation, Eq. (1), is also shown in Figure 3 (dashed line) using the same adhesion energy of $519 \, \mathrm{Nm}^{-1}$ because the adhesion energy used in the Kendall equation is defined for a peel angle $\theta = 90°$. Although the model does predict the correct trend, it increasingly overestimates the peel force as the peel angle decreases.

In addition to predicting the peel force curve, the model is also capable of predicting the change in the curvature of the backing radius, R, and the length of the peel zone, S, as a function of the peel angle, θ. Snapshot images of the peeling model tape from the borosilicate glass surface at various peel angles θ are shown in Figure 4. The solid curves and the dotted lines represent the predictions for the curvatures, using Eq. (11), and the lengths of the peel zones, using Eq. (10), respectively, both showing good agreement with the recorded images. The small variations in the lengths of the peel zone are a

A

$$S_0 = R_0 \phi_0$$

R_0

S_0

ϕ_0

1 mm

B

$\gamma = 519 \text{ N m}^{-1}$
$\phi_o = 90°$

Kendall Model
Eqn. (1)

PZ Model
Eqn. (12)

ϕ_0

Peel Force, F (Nm^{-1})

Peel angle, θ (°)

FIGURE 3 (a) Optical image of a 90° peel of the model tape. The solid and dashed lines represent the predictions of the model for the curvature of the backing and the length of the peel zone, respectively. (b) Plots of measured and theoretical peel forces *versus* peel angle for a model tape consisting of a transfer tape adhesive on a transparency film backing at a peel velocity of $v \sim 0.03$ mm/s. The solid line is the prediction of Eq. (12). The dashed line is the prediction of Eq. (1). In both cases, an adhesion energy of 519 Nm^{-1} was used as defined at $\phi_o = 90°$.

consequence of the chaotic nature of the adhesive rupture of the filaments from the glass surface, whereas the model predicts the mean (or average) length of the peel zone.

Figure 5a shows an optical image of a composite tape consisting of a layer of 3M electrical tape in addition to a layer of 3M Scotch$^{\text{TM}}$ tape peeling at $\theta = 90°$. The curvature of the backing R_o was measured to
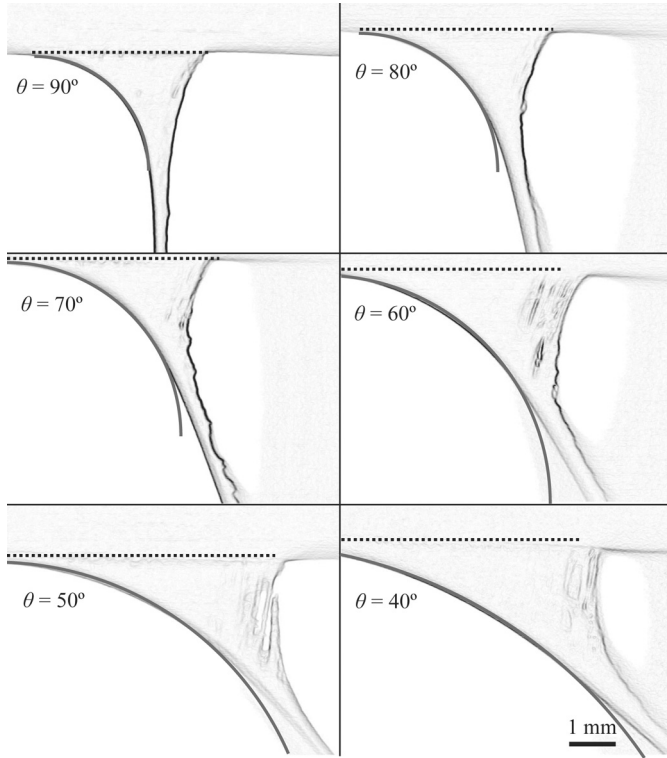
FIGURE 4 Optical images of the peel-zone region of the model tape peeling at a velocity of $v \sim 0.03$ mm/s at peel angles of $\theta = 90°, 80°, 70°, 60°, 50°,$ and $40°$. The corresponding model predictions for the curvature (solid line) and the length of the peel zone (dotted line) are superimposed on the optical images.

be 415 μm (solid curve). The active length in the peel zone, S_o, is 470 μm (dotted line). Based on the active length of the peel zone and the curvature of the backing, ϕ_o was calculated to be 65° using Eq. (9). Figure 5b is a plot of the peel force *versus* peel angle for the detachment of the tapes. A single layer of electrical tape has a low stretching modulus (*i.e.*, the tape elongates substantially even under a small tension). Thus, the model, Eq. (12) (solid curve in Figure 5b), is unable to predict correctly the peeling behavior of the tape at peel angles less than about 70° (× data points in Figure 5B). To overcome this issue, a second layer of 3M Scotch™ tape was added over the electrical tape. This modification increases the stretching modulus of the composite tape while maintaining the adhesive properties of
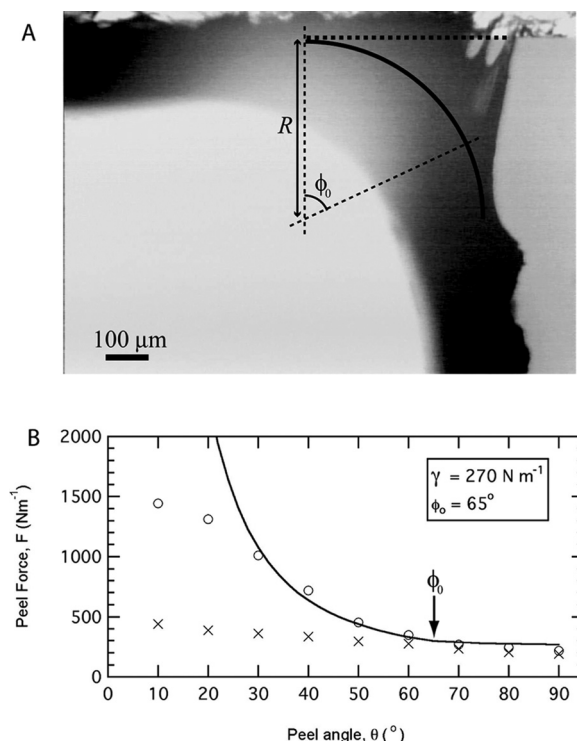
FIGURE 5 (a) Optical image of a $90°$ peel of a composite tape composed of a layer of 3M electrical tape with an additional later of 3M Scotch[TM] tape. (b) Plots of measured and theoretical peel forces *versus* peel angle for 3M electrical tape for a peel velocity of $v \sim 0.5$ mm/s. The solid line is the prediction of Eq. (12) ($\times$, data for a single layer of tape; $\bigcirc$, data for the composite tape).

the electrical tape unchanged. Using Eq. (12) with $\phi_o = 65°$, the model correctly predicts the peeling behavior of the composite tape for angles as low as $30°$ ($\bigcirc$ data points in Figure 5b). At even smaller angles, substantial stretching of the tape because of the high loads applied. The adhesion energy, as calculated from Eq. (14), gives a value of 270 Nm^{-1} defined at $\theta = 65°$.

Figure 6a shows an optical image of a composite tape consisting of two layers of 3M Scotch[TM] tape peeling at $\theta = 90°$. The value for ϕ_o was again determined from the length of the peel zone and the radius of curvature of the tape. Figure 6b is a plot of the peel force *versus* peel angle for the detachments of single and double layers
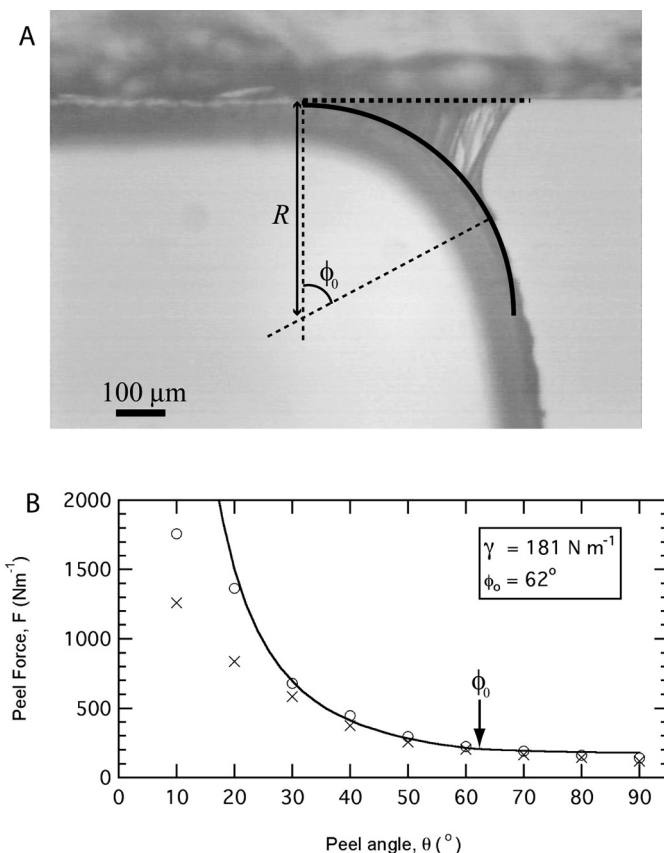
FIGURE 6 (a) Optical image of a 90° peel of the composite tape composed of two layers of 3M Scotch[TM] tape. (b) Plots of measured and theoretical peel forces *versus* peel angle for 3M Scotch[TM] tape for a peel velocity of $v \sim 0.5\,\text{mm/s}$. The solid line is the prediction of Eq. (12) ($\times$, data for a single layer of 3M Scotch[TM] tape; $\bigcirc$, data for the composite tape).

of 3M Scotch[TM] tape. A single layer of 3M Scotch[TM] tape has a relatively high stretch modulus, and the model correctly predicts the peeling behavior for angles larger than 40°. Again, at lower peel angles, significant stretching of the tape occurs. By applying a second layer of 3M Scotch[TM] tape, the stretching is diminished, and again the agreement with Eq. (12) with $\phi_0 = 62°$ is better, now down to $\theta \approx 20°$. The adhesion energy, as calculated from Eq. (14), gives a value of $181\,\text{Nm}^{-1}$ defined at $\theta = 62°$.

Application of the Model to the Gecko Adhesive System

Our model is particularly suited for application to the adhesion of geckos on surfaces due to the high elastic modulus of the keratin adhesive backing structures in the gecko: the setae, spatulae, and generally low peel angles. However, the small dimensions of gecko setae and spatulae make their forces and geometry difficult to study. Huber *et al.* [22] measured the maximum pull-off force for a single spatula to be approximately 10 nN. If each spatula on a seta can generate 10 nN, it would take approximately 4000 spatulas to generate the adhesion force of 40 μN reported by Autumn *et al.* [2] for a single seta. But, a seta contains a maximum of approximately only 1000 spatulas [37], which would give 40 nN per spatula (a factor of 4 greater than obtained by Huber *et al.*). This apparent inconsistency in the forces measured on a single spatula compared with a single seta may be due to the different methods used to measure the adhesion forces. Huber *et al.* measured the pull-off force of a spatula by pulling the seta perpendicularly from a surface, which is an analog to tape peeling at 90° at the spatula level. On the other hand, Autumn *et al.* measured the pull-off force of a seta (containing multiple spatulas) by shearing the seta as well as applying a normal force away from the surface. According to our model, the friction force produced by shearing the seta would increase the peel zone of individual spatulas, thus increasing their adhesion force. Assuming that the van der Waals forces dictate the curvature of the spatula (*i.e.*, the spatula is compliant), we can take $\phi_o \approx 90°$. Using Eq. (12) with an adhesion energy, γ, of 50 mNm^{-1} and $\phi_o = 90°$ [obtained by using Eq. (14) with $F = 10$ nN reported by Huber *et al.* and the width of a spatula $b = 200$ nm], we obtain a peel-force curve for a single spatula shown in Figure 7 (solid curve). The adhesion energy in this case is set closer to the thermodynamic surface energy due to the lack of viscoelastic adhesive fibers present in pressure-sensitive tapes. The peel angle, θ, required to yield 40 nN of normal adhesion force, $F_\perp$ (equivalent to a peel force F of about 633 mNm^{-1}), per spatula is found to be approximately 18.4°. Also shown in Figure 7 is a plot of the adhesion force calculated in our previous work [26] using a molecular level analysis (dotted curve) by considering van der Waals forces between a spatula and a surface. Because typical values were used in the molecular-level analysis, the magnitude of the peel force calculated is offset to larger values, although the analysis does predict a similar trend to that predicted by the PZ model. By multiplying the values obtained by Tian *et al.* [26] by a fitting factor of 0.55, we find a good agreement between the molecular level analysis and the PZ model for the peel force of a single spatula (dashed curve).
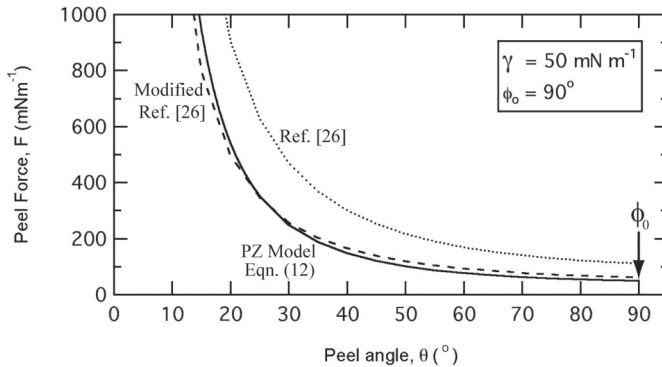
FIGURE 7 Plot of peel force *versus* peel angle for a single spatula as given by Eq. (12) using an adhesion energy of $50 \, \text{mNm}^{-1}$ as obtained by Huber *et al.* [22] and $\phi_0 = 90°$. The dotted curve is the peel force of a single spatula as a function of peel angle obtained from Ref. 26. The dashed curve is a fit of the peel force obtained from Ref. 26.

At a peel angle of $18.4°$, the component of the peel force acting parallel to the substrate (*i.e.*, the friction force) is

$$F_{\parallel} = \frac{F_{\perp}}{\tan \theta} = \frac{40 \text{ nN}}{\tan 18.4°} = 120 \text{ nN}. \tag{17}$$

The maximum *available* friction force $F_{\parallel}^{available}$ is defined as the point at which the adhering surface begins to slip (*i.e.*, the parallel component of the peel force is greater than the friction that can be provided by the adhering surfaces). $F_{\parallel}^{available}$ can be estimated by a modified Amontons' law proposed by Derjaguin [38] and is proportional to three normal force contributions but can be approximated as follows:

$$F_{\parallel}^{available} = \mu(F_{\perp}^{contact} + F_{\perp}^{noncontact} + L) \approx \mu F_{\perp}^{contact} \tag{18}$$

where μ is the coefficient of friction, $F_{\perp}^{contact}$ is the normal force in the contact region between the spatula and the surface, $F_{\perp}^{noncontact}$ is the normal force in the noncontact region [*i.e.*, the normal force within the peel zone given by Eq. (12)], and L is the applied normal load. Contribution from $F_{\perp}^{noncontact}$ and L ($\pm$weight of a gecko spread over all the spatulae pads depending whether it is on the ground or on the ceiling) are negligible compared with $F_{\perp}^{contact}$. The latter can be estimated by the van der Waals force between two flat surfaces [39] as

$$F_{\perp}^{contact} = \frac{AC_{spatula}}{6\pi D^3}, \tag{19}$$

where A is the Hamaker constant, C_{spatula} is the true contact area between the spatula and the surface, and D is the distance between the spatula and the surface. Taking $A = 1 \times 10^{-19}$ J and $D = 0.2$ nm as typical values [39], and $C_{\text{spatula}} = 4 \times 10^{-14}$ m^2 (spatulae pads are ~ 200 nm in length and width), $F_{\perp}^{contact} \approx 26$ mN. Assuming a friction coefficient of 0.25 between the spatulae pads and surface [8], $F_{\|}^{available} \approx 6.6$ mN. The available friction force is greater by more than an order of magnitude than the required $F_{\|} = 120$ nN to sustain the peel force at $18.4°$. This peel angle is also consistent with the frictional adhesion model proposed by Autumn *et al.* [8], which states that $F_{\|} \geq -F_{\perp}/\tan \alpha^*$ where α^* is the critical detachment angle of the setae. For $\alpha^* = 30°$, $1/\tan \alpha^* = 1.7$. In our case, the shear component, $F_{\|}$, is three times ($1/\tan 18.4°$) as great as the adhesion component, $F_{\perp}$, of the peel force.

A limitation of the current model is that it is unable to predict the peeling behavior of tapes with small stretch moduli or at very low peel angles, where significant stretching occurs because of the large peel forces. The stretching of the backing is expected to decrease the length of the peel zone due to filament rupture at the stationary point in the peel zone. But, in the case of the gecko adhesive system, instead of adhesive filaments dictating the curvature of a compliant backing and the adhesive force, van der Waals forces act on the spatula, so that stretching of the spatulae is not expected to change the dimensions of the peel zone significantly.

CONCLUSION

A tape-peeling model based on a static geometrical consideration of the peel zone was derived that incorporates the role of peel angle and friction on adhesion. The proposed model was tested on a model tape and two types of commercially available adhesive tapes to predict the peel force as a function of peel angle. The model accurately predicted the peel behavior for adhesive tapes with backings of high-stretch moduli. Adhesive tapes with low-stretch moduli are expected to change the shape of the peel zone and thus deviate from the proposed model. The model was applied to the gecko adhesive system and reasonably explains the apparent discrepancies in the magnitudes of the pull-off forces measured in previous experimental studies performed on different hierarchical structures of geckos.

ACKNOWLEDGMENT

REFERENCES

[1] Autumn, K., Liang, Y. A., Hsien, S. T., Zesch, W., Chan, W. P, Kenny, T. W., Fearing, R., and Full, R., *Nature* **405**, 681–685 (2000).

[2] Autumn, K., Sitti, M., Liang, Y. A., Peattie, A. M., Hansen, W. R., Sponberg, S., Kenny, T. W., Fearing, R., Israelachvili, J. N., and Full, R. J., *PNAS* **99**, 12252–12256 (2002).

[3] Yao, H. and Gao, H., *J. Mechanics Physics Solids* **54**, 1120–1146 (2006).

[4] Geim, A. K, Dubonos, S. V., Grigorieva, I. V., Novoselov, K. S., Zhukov, A. A., and Shapoval, S. Y., *Nature Materials* **2**, 461–463 (2003).

[5] Northen, M. T. and Turner, K. L., *Nanotechnology* **16**, 1159–1166 (2005).

[6] Chen, J. J., Peattie, A. M., Autumn, K., and Full, R. J., *J. Experimental Biology* **209**, 249–259 (2006).

[7] Autumn, K., Hsieh, S. T., Dudek, D. M., Chen, J., Chitaphan, C., and Full, R. J., *J. Experimental Biology* **209**, 260–272 (2006).

[8] Autumn, K., Dittmore, A., Santos, D., Spenko, M., and Cutkosky, M., *J. Experimental Biology* **209**, 3569–3579 (2006).

[9] Rivlin, R. S., *Paint Technology* **9**, 215 (1944).

[10] Kendall, K., *J. Phys. D: Appl. Phys.* **8**, 1449–1452 (1975).

[11] Gent, A. N. and Kaang, S. Y., *J. Adhes.* **24**, 173–181 (1987).

[12] Kinloch, A. J., Lau, C. C., and Williams, J. G., *Inter. J. Fracture* **66**, 45–70 (1994).

[13] Wan, K., *J. Adhes.* **70**, 197–207 (1999).

[14] Plaut, R. and Ritchie, J., *J. Adhes.* **80**, 313–331 (2004).

[15] Sato, K. and Toda, A., *J. Phys. Soc. Jpn.* **73**, 2135–2141 (2004).

[16] Sun, Z., Wan, K., and Dilliard, D. A., *Inter. J. Solids Structures* **41**, 717–730 (2004).

[17] Williams, J. A. and Kauzlarich, J. J., *Tribology International* **38**, 951–958 (2005).

[18] Ciccotti, M., Giorgini, B., Vallet, D., and Barquins, M., *Inter. J. Adhes. Adhesives* **24**, 143–151 (2004).

[19] Newby, B. Z. and Chaudhury, M. K., *Langmuir* **14**, 4865–4872 (1998).

[20] Persson, B. N. J. and Gorb, S., *J. Chem. Phys.* **119**, 11437–11444 (2003).

[21] Spolenak, R., Gorb, S., Gao, H. J., and Arzt, E., *Proc. R. Soc. Lond. Ser. A: Math. Phys. Eng. Sci.* **461**, 305–319 (2004).

[22] Huber, G., Gorb, S. N., Spolenak, R., and Arzt, E., *Biol. Lett.* **1**, 2–4 (2005).

[23] Hansen, W. and Autumn, K., *PNAS* **102**, 385–389 (2005).

[24] Newby, B. Z., Chaudhury, M. K., and Brown, H. R., *Science* **269**, 1407–1409 (1995).

[25] Amouroux, N., Petit, J., and Léger, L., *Langmuir* **17**, 6510–6517 (2001).

[26] Tian, Y., Pesika, N. S., Zeng, H., Rosenberg, K., Zhao, B., McGuiggan, P., Autumn, K., and Israelachvili, J., *PNAS* **103**, 19320–19325 (2006).

[27] Zosel, A., *J. Adhes.* **30**, 135–149 (1989).

[28] Zosel, A., *Int. J. Adhes. Adhesives* **18**, 265–271 (1998).

[29] Créton, C. and Leibler, L., *J. Polym. Sci. B: Polym. Phys.* **34**, 545–554 (1996).

[30] Lindner, A., Maevis, T., Brummer, R., Luhmann, B., and Créton, C., *Langmuir* **20**, 9156–9169 (2004).

[31] Shull, K. R. and Créton, C., *J. Polym. Sci. B: Polym. Phys.* **42**, 4023–4043 (2004).

[32] Brown, K., Hooker, J. C., and Créton, C., *Macromol. Mat. Eng.* **287**, 163–179 (2002).

[33] Lindner, A., Lestriez, B., Mariot, S., Créton, C., Maevis, T., Luhmann, B., and Brummer, R., *J. Adhes.* **82**, 267–310 (2006).

[34] Créton, C., Hooker, J., and Shull, K. R., *Langmuir* **17**, 4948–4954 (2004).

[35] Portigliatti, M., Koutsos, V., Hervet, H., and Léger, L., *Langmuir* **16**, 6374–6376 (2000).

[36] Autumn, K., Majidi, C., Groff, R. E., Dittmore, A., and Fearing, R., *J. Experimental Biology* **209**, 3558–3568 (2006).

[37] Ruibal, R. and Ernst, V., *J. Morphology* **117**, 271–294 (1965).

[38] Derjaguin, B. V., *Z. Phys.* **88**, 661 (1934).

[39] Israelachvili, J. N., *Intermolecular Surface Forces* (Elsevier Academic Press, San Diego, 2005), 2nd ed., Chap. 11, pp. 176–179.